Materials Science & Engineering C 85 (2018) 7–17

Contents lists available at ScienceDirect

Materials Science & Engineering C

journal homepage: www.elsevier.com/locate/msec

Biodistribution and preliminary toxicity studies of nanoparticles made of Biotransesterified β–cyclodextrins and PEGylated phospholipids

P. Perret[a], S. Bacot[a], A. Gèze[b], A. Gentil Dit Maurin[b], M. Debiossat[a], A. Soubies[a], V. Blanc-Marquis[b], L. Choisnard[b], J. Boutonnat[c], C. Ghezzi[a], J.L. Putaux[d], C. Lancelon-Pin[d], L.M. Riou[a,*], D. Wouessidjewe[b]

[a] INSERM, UMR 1039, Radiopharmaceutiques Biocliniques, Grenoble-Alpes University, France
[b] DPM, UMR CNRS 5063, ICMG FR 2607, Faculty of Pharmacy, Grenoble-Alpes University, France
[c] CHU Grenoble-Alpes - TIMC UMR CNRS 5525, France
[d] CERMAV-CNRS, UPR 5301, ICMG FR 2607, Grenoble-Alpes University, France

ARTICLE INFO

Keywords:
Bioesterified β-cyclodextrins
PEGylated amphiphiles
Nanoparticles
Biodistribution
Toxicity studies

ABSTRACT

Background: The modification of β-cyclodextrins (βCDs) by grafting alkyl chains on the primary and/or secondary face yields derivatives (βCD-C10) able to self-organize under nanoprecipitating conditions into nanoparticles (βCD-C10-NP) potentially useful for drug delivery. The *co*-nanoprecipitation of βCD-C10 with polyethylene glycol (PEG) chains yields PEGylated NPs (βCD-C10-PEG-NP) with potentially improved stealthiness. The objectives of the present study were to characterize the *in vivo* biodistribution of βCD-C10-PEG-NP with PEG chain length of 2000 and 5000 Da using nuclear imaging, and to preliminarily evaluate the *in vivo* acute and extended acute toxicity of the most suitable system.

Research design and methods: The *in vivo* and *ex vivo* biodistribution features of naked and decorated nanoparticles were investigated over time following intravenous injection of ^{125}I-radiolabeled nanoparticles to mice. The potential toxicity of PEGylated βCD-C10 nanosuspensions was evaluated in a preliminary *in vivo* toxicity study involving blood assays and tissue histology following repeated intraperitoneal injections of nanoparticles to healthy mice.

Results: The results indicated that βCD-C10-PEG$_{5000}$-NP presented increased stealthiness with decreased *in vivo* elimination and increased blood kinetics without inducing blood, kidney, spleen, and liver acute and extended acute toxicity.

Conclusions: βCD-C10-PEG$_{5000}$-NPs are stealth and safe systems with potential for drug delivery.

1. Introduction

Nanomedicine is an emerging sector of nanotechnology with a variety of nanoscale systems in clinical use or under development for diagnostic and therapeutic purposes [1–3]. Various materials are considered for the design of nanoconstructs. Among them, cyclodextrins (CDs) are well-known cyclic oligosaccharides obtained by glucosyltransferase degradation of starch [4]. The parent cyclodextrin series is constituted of 6 (αCD), 7 (βCD) or 8 (γCD) D-glucopyranoside units linked by α(1,4) bonds. Parent and modified cyclodextrins have been widely used as pharmaceutical excipients and applied through various routes of administration to formulate drugs with poor bioavailability. Indeed, CDs have been shown to improve the apparent aqueous solubility and/or stability of the guest molecule by forming drug/CD inclusion complexes [5–10]. In the setting of rapidly developing nanomedicine, important chemical manipulations were performed on CDs to design amphiphilic CD monomers able to form drug nanocarriers with sufficient stability in the presence of biological fluids [11–13]. Specifically, the modification of cyclodextrins (CDs) by grafting alkyl chains on the primary and/or secondary face either *via* chemical or enzymatic pathways yielded derivatives able to self-organize into nanodevices potentially useful for drug delivery [14,15]. CD derivatives bearing alkyl chains (C6 to C14) on the secondary hydroxyl groups are currently developed by our group and involve vinyl esters as alkyl donors and thermolysin as a biocatalyzer [16]. These CD derivatives have been shown to nano-assemble under nanoprecipitation conditions (also called solvent displacement method), forming nanoparticles with various morphologies [17]. The α-, β- and γ-CD-10 nanoparticles have

* Corresponding author at: INSERM, U1039 Radiopharmaceutiques Biocliniques, Faculté de Médecine de Grenoble, F-38700 La Tronche, France.
E-mail address: Laurent.Riou@univ-grenoble-alpes.fr (L.M. Riou).

https://doi.org/10.1016/j.msec.2017.12.017
Received 7 July 2017; Received in revised form 13 September 2017; Accepted 7 December 2017
Available online 15 December 2017

been proved to associate bioactive substances and release them *in vitro* or *in vivo* [18–20]. The co-nanoprecipitation of bio-esterified γ-CD-C10 with PEGylated amphiphiles (PEG esters, polysorbate 80) was investigated by our group and provided an interesting way to obtain surface-modified nanoparticles. The co-nanoprecipitation methodology was then extended to the use of PEGylated phospholipids (PEG) with a molecular weight of 2000 Da. The surface decorated colloids were evaluated *in vitro* as well as *in vivo* for their hemolytic and stealthy performance using fluorescence imaging. We demonstrated that decorating the surface of γ-CD-C10-based nanospheres with DMPE-PEG_{2000} might allow better protection against plasma protein absorption and therefore improved blood kinetics in mice. These nanoparticles also proved to be non-hemolytic at the concentration range used *in vivo* [21].

The β-CD-C10 derivative is currently intensively studied as well for its potential in drug delivery due to its strong ability to nano-assemble into small-size nanoparticles presenting original supramolecular organizations such as onion-like and hexagonal structures [16,22], which provide the opportunity to associate hydrophilic or lipophilic drugs. In the present study, the concept of co-nanoprecipitation was applied to biosynthesized β-CD-C10 derivative using PEGylated phospholipids with PEG chain lengths of 2000 and 5000 Da in order to test the hypothesis of increased stealthiness with increasing PEG chain length. The *in vivo* and *ex vivo* biodistribution features of naked and decorated nanoparticles were therefore investigated over time following intravenous (iv) injection of ^{125}I-radiolabeled nanoparticles to mice. In addition and considering the extremely encouraging results observed with PEG_{5000}-decorated NPs, the questions of the potential toxicity of PEGylated β-CD-C10 nanosuspensions was also addressed in a preliminary *in vivo* toxicity study involving blood assays and tissue histology following repeated intraperitoneal injections of nanoparticles to healthy mice.

2. Materials & methods

2.1. βCD-C10 radiolabeling and ^{125}I-βCD-C10-based nanoparticle (NP) formulation

A summary of the experimental conditions used for βCD-C10 radiolabeling and ^{125}I-βCD-C10-NP, ^{125}I-β-CD-C10-PEG_{2000}-NP, and ^{125}I-βCD-C10-PEG_{5000}-NP formulation is provided in Table 1 and Fig. 1 below.

2.1.1. Synthesis of βCD-C10 and I-βCD-C10

βCD-C10 fatty ester was synthesized in our laboratory from parent βCD (Kleptose®, Roquette Frères, France) by enzymatically assisted pathway using thermolysin (EC 3.4.24.27 [Sigma- Aldrich], a protease type X isolated from *Bacillus thermoproteolyticus rokko*) as catalyzer and decanoic vinyl esters (C10) (vinyl decanoate, Sigma-Aldrich) as acyl donors according to a procedure previously described by Choisnard et al. [16,22]. The product, obtained as a white powder, was characterized by an average molecular weight of 2266 g·mol^{-1} corresponding to a total degree of substitution (TDS) of 7.3 [40]. Concerning the iodinated βCD-C10, a similar procedure was used from the periodinated βCD in primary face (heptakis-6-iodo-6-deoxy-beta-cyclodextrin, Acros Organics, France). The synthesized powder was characterized by an average molecular weight of 2505 g·mol^{-1}, corresponding to a TDS of 3.9.

2.1.2. Radiolabeling of βCD-C10

The labeling was performed by ^{125}I/^{127}I isotopic exchange as described by Gèze et al. [23] and optimized as follows: 1 mg of unlabeled ^{127}I-βCD-C10 was dissolved into 1 mL of acetone before being added to 3 μg of a solution of $Na^{127}I$ (1 mg·mL^{-1} in acetone) and 140 MBq of $Na^{125}I$. The mixture was incubated at 95–100 °C for 105 min. Radiochemical purity (RCP) was determined by thin-layer chromatography (TLC) on RP-18 silica gel (stationary phase) using physiological serum (PS) as the mobile phase after depositing a drop of the radiolabeled solution at 2 cm from the origin of the chromatographic support. A ScanRam radioTLC Detector was used for TLC plate analysis. The retardation factor (Rf) was determined as the ratio of the radioactive material distance of migration to the mobile phase distance of migration. The RCP of ^{125}I-labeled-βCD-C10 was also evaluated up to 72 h post-radiolabeling at 4 °C using the above mentioned conditions in order to determine stability over time (n = 2–3/time point).

2.1.3. Nanoparticle formulation

βCD-C10-based nanosphere suspensions were prepared using the solvent displacement technique as described elsewhere [18]. Briefly, the method consisted in injecting, under magnetic stirring (500 rpm) at 25 °C, an organic solution (anhydrous acetone, HPLC grade) containing βCD-C10 (1 mg·mL^{-1}), into distilled water (freshly made in our laboratory). The acetone/water volume ratio was set at 1/3. Nanoparticles (βCD-C10-NPs) spontaneously formed and the organic solvent was then removed at 40 °C. The suspensions were concentrated until a final aqueous volume representing 70–80% of the initial distilled water volume. The aqueous suspensions were filtered through 0.8 μm (CME filters, Roth Sochiel, France). Iodinated nanoparticles were obtained in a similar way using an acetone solution containing a mixture of a mass ratio of I-βCD-C10/βCD-C10 fixed at 1/1.

PEGylated βCD-C10-NPs were obtained in a similar way by co-nanoprecipitating either a mixture of βCD-C10 or (βCD-C10/I-βCD-C10) and PEGylated phospholipid. The latter was either DMPE-$mPEG_{2000}$ (1,2-dimyristoyl-sn-glycero-3-phosphoethanolamine-N-[carbonyl-methoxypolyethylene glycol-2000, MW ≈ 2800 g·mol^{-1}]) or DSPE-

Table 1
Preparation parameters and characteristics of ^{125}I-βCD-C10-NP, 125I-βCD-C10-PEG_{2000}-NP, and ^{125}I-βCD-C10-PEG_{5000}-NP.

	βCD-C10-NP		^{125}I-βCD-C10-NP		^{125}I-βCD-C10-PEG_{2000}-NP		^{125}I-βCD-C10-PEG_{5000}-NP	
	(10^{-2} g)	mol	(10^{-3} g)	mol	(10^{-3} g)	mol	(10^{-3} g)	mol
β-I-CD-C10	–	–	1.0	4.0E − 07	1.0	4.0E − 07	0.9	3.6E − 07
β-CD-C10	2.0	8.8E − 07	1.0	4.4E − 07	1.0	4.4E − 07	1.1	4.7E − 07
DMPE-$mPEG_{2000}$	–	–	–		1.0	3.6E − 07	–	
DSPE-$mPEG_{5000}$	–	–	–		–		3.0	5.0E-07
Total formulated mass	2		2.0		3.0		5.0	
Final volume (mL)	5.2		5.2		5.3		4.2	
Final activity (MBq)	–		112.5		92.5		108.4	
Nanoparticle PI	0.12 ± 0.05		[a]0.11 ± 0.04		[a]0.24 ± 0.07		[a]0.20 ± 0.06	
Nanoparticle Dh (nm)	51 ± 5		[a]54 ± 5		[a]63 ± 5		[a]69 ± 6	
Nanoparticle ζ (mV)	− 21 ± 2		[a]-24 ± 2		[a]-20 ± 2		[a]-14 ± 3	

Dh: hydrodynamic diameter, ζ: zeta potential, PI: polydispersity index.
[a] The determination of Dh, PI, and ζ values (mean ± standard deviation of eight different batches of nanoparticle suspensions) was performed on separate experiments with non-radiolabeled iodinated NP.

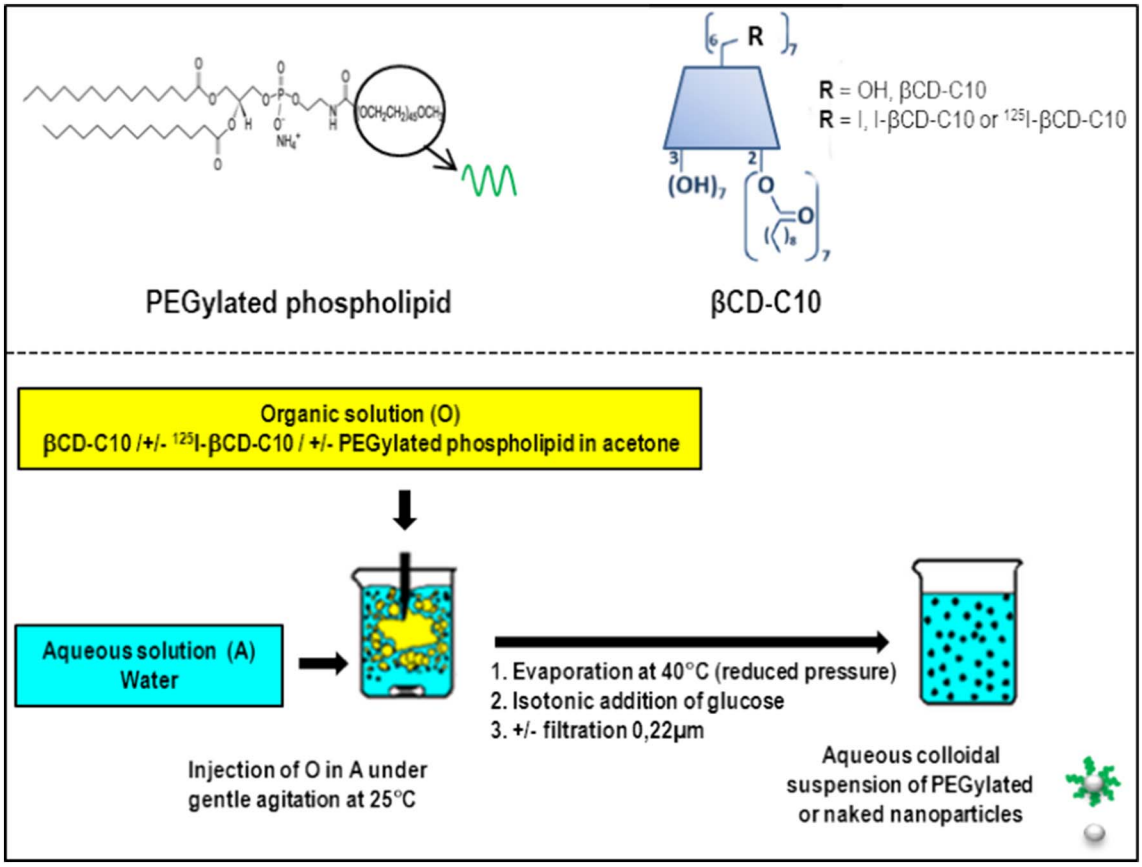

Fig. 1. Main steps allowing the formation of ^{125}I-βCD-C10-NP. See text for details.

mPEG$_{5000}$ (1,2-distearoyl-sn-glycero-3-phosphoethanolamine-N-[carbonyl-methoxypolyethylene glycol-5000], $M_W \approx 5900\ g{\cdot}mol^{-1}$) both supplied by Corden Pharma (Switzerland). Both amphiphiles were solubilized in acetone prior to injection in water phase. βCD-C10 ± I-βCD-C10/PEGylated phospholipid mass ratios of 2/1 and 2/3 were used for DMPE-PEG$_{2000}$ and DSPE-PEG$_{5000}$, respectively. Each formulation was made in triplicate, immediately characterized and was stored at room temperature in sealed vials for stability studies. The radiolabeled (^{125}I) nanoparticles were prepared in a dedicated room, in a sealed enclosure according to the same methodology by replacing ^{127}I-βCD-C10 by ^{125}I-βCD-C10 (See Subsection 2.1.2 above).

The suspensions intended for *in vivo* studies were rendered isotonic with a sterile glucose solution. In the case of the toxicity study, the colloidal DSPE-mPEG$_{5000}$/βCD-C10 suspensions (namely βCD-C10-PEG$_{5000}$-NP) were filtered through sterile 0.22 µm filters, and stored in autoclaved glass vials before administration to animals.

2.1.4. Physicochemical characterization of the nanosystems

The mean size (Dh), polydispersity index (PI) and zeta potential were determined after appropriate dilution using a Zetasizer (Nano ZS, Malvern Instruments). The nanosystems were observed by transmission electron microscopy (TEM) after negative staining of the preparations with 2 wt% uranyl acetate, using a Philips (FEI) CM200 microscope operating at 80 kV or 200 kV. The images were recorded on Kodak SO163 films or with a TVIPS TemCam F216 digital camera. The osmolarity was also measured in triplicate with a Loser Messtechnik type 15 automatic micro-osmometer.

2.2. Biodistribution studies

All experimental procedures were performed in accordance with institutional and EU (directive 2010/63/EU) guidelines and approved by the Animal Care and Use committee of Grenoble-Alpes University.

2.2.1. Experimental protocol

Fifty-one (51) CD1 female mice (mean weight, 23.9 ± 0.3 g) (Charles River Laboratories, France) were used for biodistribution studies. Conscious animals were injected under light constraint with the radiotracers ^{125}I-βCD-C10-NP (n = 17), ^{125}I-βCD-C10-PEG$_{2000}$-NP (n = 17), or ^{125}I-βCD-C10-PEG$_{5000}$-NP (n = 17) in a caudal vein. The mean injected dose of radiolabeled nanoparticles used for biodistribution studies was 2.23 ± 0.05 MBq (82 ± 6 µg)/animal (0.10 ± 0.00 MBq·g^{-1} of body weight). Euthanasia was performed using carbon dioxide inhalation at 10 min (n = 3/radiotracer), 1 h (n = 3/radiotracer), 3 h (n = 3/radiotracer), 6 h (n = 3/radiotracer), and 24 h (n = 5/radiotracer) following intravenous injection of ^{125}I-βCD-C10-NP, ^{125}I-βCD-C10-PEG$_{2000}$-NP, or ^{125}I-βCD-C10-PEG$_{5000}$-NP. Two animals from the 24 h time point were dedicated to longitudinal noninvasive *in vivo* single photon emission computed tomography (SPECT) imaging at 10 min, 1 h, 3 h, 6 h, and 24 h following ^{125}I-βCD-C10-NP (n = 2), ^{125}I-βCD-C10-PEG$_{2000}$-NP (n = 2), or ^{125}I-βCD-C10-PEG$_{5000}$-NP (n = 2) intravenous injection. These animals were injected with 4.8 ± 0.2 MBq of each radiotracer (0.18 ± 0.01 MBq·g^{-1} of body weight) in order to increase count statistics during SPECT image acquisitions.

2.2.2. Noninvasive in vivo SPECT imaging

Mice (n = 2 per radiotracer, see above) were anesthetized with 1.5% isoflurane in a 1:1 mixture of room air:oxygen and were then placed in a temperature-controlled bed for whole-body SPECT/CT acquisitions (nanoSPECT; Bioscan/Mediso). Helicoidal SPECT acquisition was first performed with 4 heads equipped with multipinhole collimators (9 × 1.4-mm-diameter pinholes/head) using 24 projections. Then, a 10-min-long X-ray computed tomography (CT) acquisition was

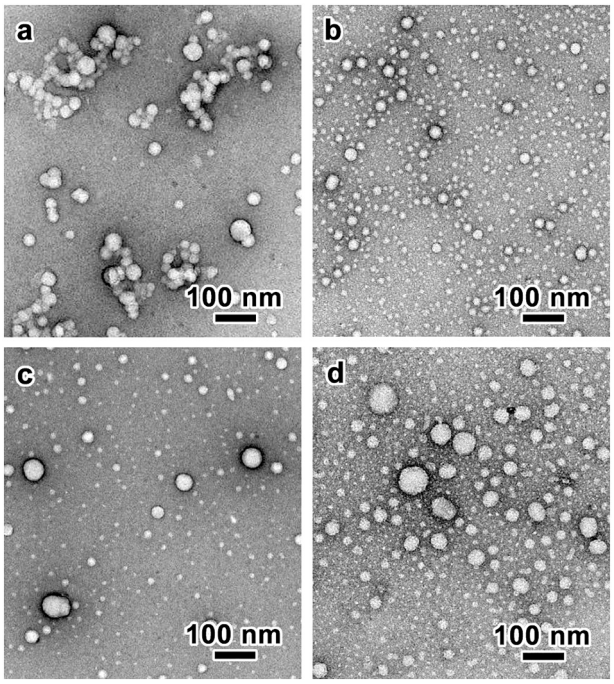

Fig. 2. Transmission electron microscopy (TEM) images of nanocarriers. TEM images of negatively stained I-βCD-C10-NPs (a), I-βCD-C10-PEG2000-NPs (b), I-βCD-C10-PEG5000-NPs (c), and βCD-C10-PEG5000-NPs (toxicity study) (d).

performed using the following acquisition parameters: 45 kVp, 240 projections, and 500 ms per projection. SPECT and CT acquisitions were reconstructed and fused using dedicated software (InVivoScope; inviCRO, LLC).

2.2.3. Organ withdrawal

Samples from the following organs and tissues were carefully harvested following euthanasia as described above: blood, liver, kidney, spleen, bile, brain, heart, stomach, salivary gland (SG), white adipose tissue (WAT), brown adipose tissue (BAT), intestine, skeletal muscle, skin, pancreas, lung, and thyroid. The samples were quickly rinsed with saline when applicable and weighed prior to the assessment of radioactivity using a gamma-well counter (Wizard^2, PerkinElmer). Radiotracer organ or tissue activity was expressed as percentage of injected dose (%ID) or Differential Uptake Ratio (DUR). %ID values were determined assuming previously published organ weight for animals similar to those used in the present study [24]. DUR is defined as (organ sample activity/organ sample weight)/(total injected activity/animal body weight) with activities and weights expressed in MBq and g, respectively. Area under the curve (AUC) values were determined for ^{125}I-βCD-C10-NP, ^{125}I-βCD-C10-PEG$_{2000}$-NP, or ^{125}I-βCD-C10-PEG$_{5000}$-NP blood and spleen activities using a logarithmic and a linear method, respectively.

2.3. Preliminary toxicity studies

2.3.1. Animals

Twenty-five (25) CD1 female mice (mean weight, 30.6 ± 0.9 g) (Charles River Laboratories, France) were used for preliminary toxicity studies. The animals were housed (4–5 animals/cage) in an environmentally controlled room with a 12 h light/dark cycle and with free access to a standard laboratory diet (Serlab) and water. Animals were allocated to two experimental groups. All animals were injected intraperitoneally, three times per week for two weeks, with βCD-C10-PEG$_{5000}$-NP (βCD-C10-PEG$_{5000}$-NP group, n = 12, 2.6 mg·mL^{-1}, 0.3 mL 780 μg/injection, ~4.68 mg total) or with physiological serum 5% glucose (CTL group, n = 13, 0.3 mL/injection). Animals were euthanized at either day 3 (βCD-C10-PEG$_{5000}$-NP group, n = 8; CTL group, n = 8) or day 30 (βCD-C10-PEG$_{5000}$-NP group, n = 4; CTL group, n = 5) following treatment completion. Animal weight was monitored thrice a week throughout the study.

Table 2
Radiochemical purity values (RCP) of ^{125}I-βCD-C10, ^{125}I-βCD-C10-NP, ^{125}I-βCD-C10-PEG$_{2000}$-NP, and ^{125}I-βCD-C10-PEG$_{5000}$-NP.

	RCP (%)
^{125}I-βCD-C10	
0 h	98.3 ± 0.3
24 h	98.6 ± 0.0
48 h	97.5 ± 0.7
72 h	97.2 ± 0.8
^{125}I-βCD-C10-NP	
0 h	95.4
6 h	95.1
24 h	94.7
^{125}I-βCD-C10-PEG$_{2000}$-NP	
0 h	92.3
6 h	96.7
24 h	94.4
^{125}I-βCD-C10-PEG$_{5000}$-NP	
0 h	92.6
6 h	97.6
24 h	93.6

^{125}I-βCD-C10 RCP values were expressed as mean ± SD of 2–3 experiments. Single values obtained upon the day of the experiment are presented for ^{125}I-βCD-C10-NP, ^{125}I-βCD-C10-PEG$_{2000}$-NP, and ^{125}I-βCD-C10-PEG$_{5000}$-NP.

2.3.2. Experimental protocol

The animals were anesthetized with an intraperitoneal injection of a 1:2 mixture of xylazine (20 mg·mL^{-1}): ketamine (100 mg·mL^{-1}) (1 μL·g^{-1}). A thoracotomy was performed for intracardiac blood collection (~0.5 mL). Whole blood samples were used for the determination of hematocrit using a Hawksley Hematocrit Centrifuge (Hema-C, Jouan) and Hawksley Micro-Hematocrit Reader as well as for the determination of erythrocyte, leukocyte, and thrombocyte cell counts using kits from Bioanalytic GmbH (Umkirch, Germany) and respective blood dilutions of 1/200, 1/20, and 1/20 in accordance with the manufacturer's instructions.

Serum was obtained from whole blood through centrifugation (3000 g/10 min/4 °C) and used for the determination of serum creatinine concentration and alanine aminotransferase (ALT) enzymatic activity using a MAK080 kit (Sigma-Aldrich) and a MAK052 kit (Sigma-Aldrich), respectively. Creatinine concentration and ALT activity were determined by coupled enzyme reaction, which results in a colorimetric product. In the case of creatinine, the amount of colorimetric product being generated is directly proportional to the amount of creatinine. In the case of ALT, 1 unit of enzyme was defined as the amount of enzyme that generated 1 μmole of pyruvate per minute at 37 °C. The amount of pyruvate being generated was proportional to the amount of colorimetric product as well. Measurements were performed at 560 nm for each assay using a Thermo Multiskan Ex and dedicated software (Ascent Software for Multiskan). In addition, the brain, heart, kidneys, liver, ovaries and spleen were quickly withdrawn upon euthanasia, rinsed, weighed and fixed in formaldehyde 4% (pH 6.9) for 24 h.

2.3.3. Histological staining

Formaldehyde-fixed tissues were included in paraffin using dedicated automates (Automatic Tissue Processor, Leica TP1020 and Heated Paraffin Embedding Module, Leica EG1150H). Four (4) to 5 μm-thick cohesive sections of paraffin-embedded tissues were obtained using a semi-automated Rotary Microtome (Leica RM2245) and placed on poly-lysine coated slides (Thermo Scientific). HES (Hematoxylin, Eosin, Saffron) staining was then performed using a Leica Autostainer XL.

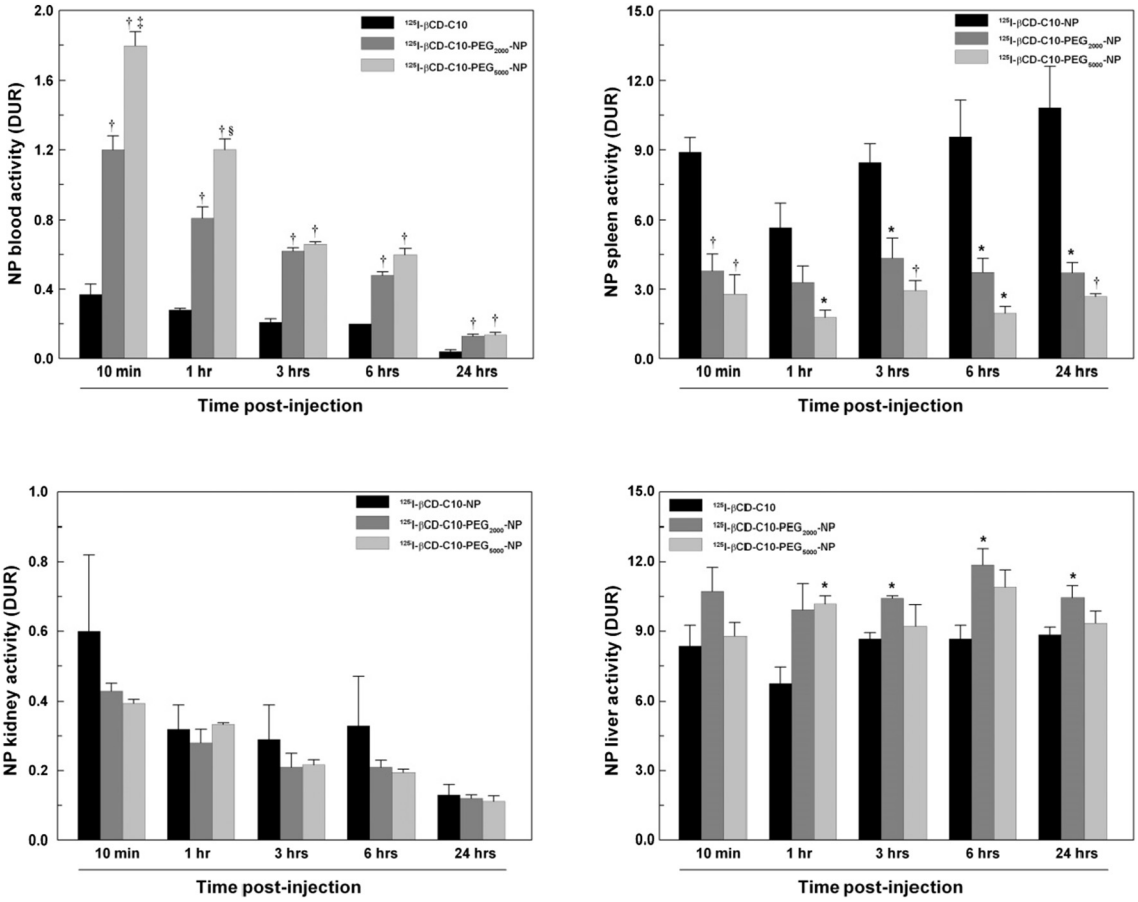

Fig. 3. *Ex vivo* biodistribution of nanocarriers. Blood, spleen, kidney, and liver activity of ^{125}I-βCD-C10, ^{125}I-βCD-C10-PEG$_{2000}$, and ^{125}I-βCD-C10-PEG$_{5000}$ at 10 min, 1 h, 3 h, 6 h, and 24 h following intravenous injection in conscious mice. * and †, $P < 0.05$ and $P < 0.01$, respectively, *vs.* ^{125}I-βCD-C10; ‡ and §, $P < 0.05$ and $P < 0.01$, respectively, *vs.* ^{125}I-β-CD-C10-PEG$_{2000}$.

Digital images of stained tissues were obtained using an Olympus BX51 and dedicated software (Leica Application Suite 3.6.0). Blinded analysis of stained histological sections was performed by an anatomopathologist (JB).

2.4. Statistical analysis

Results are presented as mean ± standard error of the mean (sem). Within- and between-group statistical analysis was performed using paired- and unpaired *t*-test, respectively. *P* values < 0.05 were considered statistically significant.

3. Results

3.1. Physico-chemical characterization of βCD-C10 based colloidal carriers

Table 1 above summarizes the characteristics of the βCD-C10-NP, ^{125}I-βCD-C10-NP, ^{125}I-βCD-C10-PEG$_{2000}$-NP and ^{125}I-βCD-C10-PEG$_{5000}$-NP.

The reported mean size (~50 nm) and zeta potential values (− 22 mV) of βCD-C10-NP and ^{125}I-βCD-C10-NP were quite similar. Both colloidal suspensions were monodisperse and displayed narrow distribution with polydispersity indexes of 0.11 and 0.12, respectively. The introduction of PEGylated phospholipids in the formulation step induced a slight increase in the average diameter of nanoparticles, which was more pronounced in the case of 5 kDa PEG chain length with a 15 nm shift. In addition, absolute zeta potential values decreased with increasing PEG chain length (I-βCD-C10-NP, − 24 mV; I-βCD-C10-PEG$_{2000}$-NP, − 20 mV; I-βCD-C10-PEG$_{5000}$-NP, − 14 mV).

The βCD-C10-PEG$_{5000}$-NP used for preliminary toxicity studies had a hydrodynamic diameter of 66 ± 2 nm and a zeta potential of − 15 ± 2 mV.

Beside nanoparticle size and electric charge, the colloidal stability of all extemporaneously prepared βCD-C10 nanoparticle suspensions was tested in electrolyte medium (0.09% NaCl). This visual test revealed that the I-βCD-C10-NP showed a poor colloidal stability associated with rapid flocculation. On the contrary, the I-βCD-C10-PEG$_{2000}$-NP and I-βCD-C10-PEG$_{5000}$-NP displayed satisfying colloidal stability (results not shown). Corresponding TEM micrographs of negatively stained formulations are shown in Fig. 2. In all cases, nanoparticles had a spheroidal shape. I-βCD-C10-NP presented mild aggregation that was not reflected in the DLS values (Fig. 2a). A preparation artefact is most likely as it has been previously shown that the negative stain could promote the aggregation of amphiphilic βCD nanoparticles upon drying [25]. The presence of PEGylated lipids in the formulation clearly prevented such an artefact as the negatively stained nanoparticles were well dispersed on the supporting carbon film (Fig. 2b, c and d).

3.1.1. Radiolabeling of βCD-C10

As shown in Table 2 below, ^{125}I-βCD-C10 (Rf = 0 as determined from TLC analysis) was successfully radio-iodinated with high RCP (> 97%) thereby obviating the need for purification. As expected, free ^{125}I (< 3%) was found at Rf = 1. The labeling efficiency corresponding to ^{125}I-exchange yield was therefore > 95%. An excellent stability of ^{125}I-βCDs (RCP > 95%) was observed up to 72 h following radiolabeling.

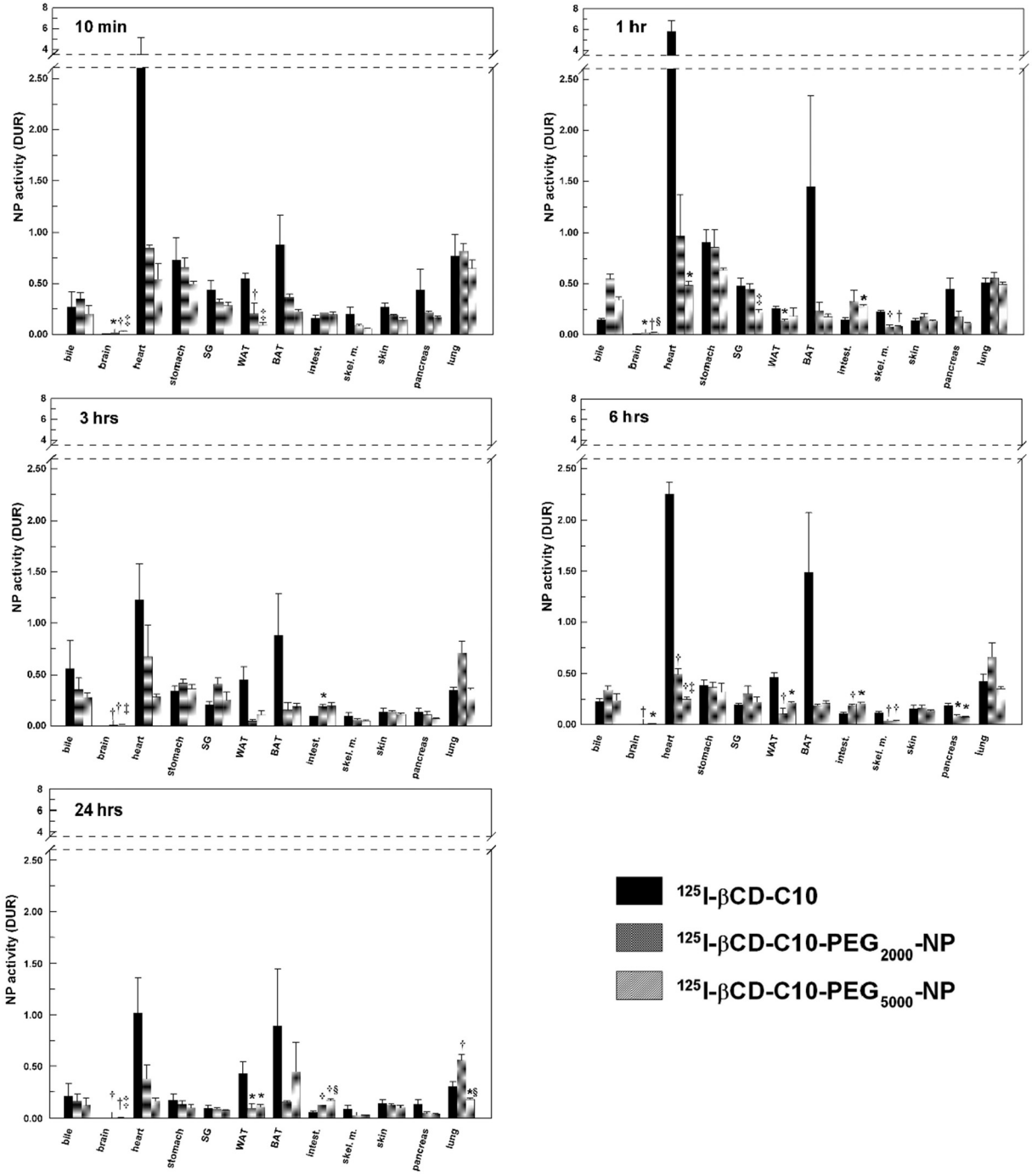

Fig. 4. *Ex vivo* biodistribution of nanocarriers. Organ biodistribution of ^{125}I-βCD-C10, ^{125}I-βCD-C10-PEG$_{2000}$, and ^{125}I-βCD-C10-PEG$_{5000}$ at 10 min, 1 h, 3 h, 6 h, and 24 h following intravenous injection in conscious mice. SG, salivary glands; WAT, white adipose tissue; BAT, brown adipose tissue; intest., intestine; skel. m., skeletal muscle. * and †, $P < 0.05$ and $P < 0.01$, respectively, *vs* ^{125}I-βCD-C10; ‡ and §, $P < 0.05$ and $P < 0.01$, respectively, *vs*. ^{125}I-βCD-C10-PEG$_{2000}$.

3.1.2. Preparation of radiolabeled ^{125}I-βCD-C10-NP, ^{125}I-βCD-C10-PEG$_{2000}$-NP, and ^{125}I-βCD-C10-PEG$_{5000}$-NP

The absence of free ^{125}I in the ^{125}I-βCD solutions was confirmed by TLC before each co-nanoprecipitation procedure. TLC profiles indicated a minor peak at Rf = 1 corresponding to free ^{125}I (< 5%), while ^{125}I-βCD-C10-NP, ^{125}I-βCD-C10-PEG$_{2000}$-NP, and ^{125}I-βCD-C10-PEG$_{5000}$-NP did not migrate (Rf = 0). The radiochemical purities of ^{125}I-βCD-C10-NP, ^{125}I-βCD-C10-PEG$_{2000}$-NP, and ^{125}I-βCD-C10-PEG$_{5000}$-NP upon formulation were 95.4, 95.1 and 94.7%, respectively. ^{125}I-βCD-C10-NP, ^{125}I-βCD-C10-PEG$_{2000}$-NP, and ^{125}I-βCD-C10-PEG$_{5000}$-NP stability was evaluated by TLC at 6 h and 24 h post-formulation with no significant degradation being observed (respective RCPs, 92.3, 96.7, 94.4% at 6 h and 92.6, 97.6, and 93.6% at 24 h). Small amounts of by-products with intermediary Rf were observed, which were considered negligible (Table 2).

3.2. Biodistribution studies

The comparison of blood, spleen, kidney and liver biodistributions of ^{125}I-βCD-C10-NP, ^{125}I-βCD-C10-PEG$_{2000}$-NP, and ^{125}I-βCD-C10-PEG$_{5000}$-NP from 10 min to 24 h following intravenous injection are shown in Fig. 3. The results indicated a graded increase in circulating nanoparticle blood activity from ^{125}I-βCD-C10-NP to ^{125}I-βCD-C10-PEG$_{2000}$-NP and ^{125}I-βCD-C10-PEG$_{5000}$-NP with significant differences

Table 3
^{125}I-βCD-C10-NP, ^{125}I-βCD-C10-PEG$_{2000}$-NP, and ^{125}I-βCD-C10-PEG$_{5000}$-NP activities in major organs following intravenous injection.

	Time post-injection (h)				
Organ activity (%ID)	0.16	1	3	6	24
Blood					
^{125}I-βCD-C10-NP	2.67 ± 0.48	2.25 ± 0.08	1.55 ± 0.16	1.51 ± 0.03	0.30 ± 0.03
^{125}I-βCD-C10-PEG$_{2000}$-NP	8.97 ± 1.12*	6.33 ± 0.29†	4.31 ± 0.15†	3.55 ± 0.12†	0.89 ± 0.05†
^{125}I-βCD-C10-PEG$_{5000}$-NP	12.64 ± 0.90†	8.49 ± 0.63†‡	4.35 ± 0.12†	4.02 ± 0.23†	0.89 ± 0.10†
Spleen					
^{125}I-βCD-C10-NP	3.73 ± 0.23	2.65 ± 0.46	3.61 ± 0.29	4.29 ± 0.73	4.49 ± 0.74
^{125}I-βCD-C10-PEG$_{2000}$-NP	1.64 ± 0.30†	1.55 ± 0.38	1.81 ± 0.44*	1.62 ± 0.29	1.53 ± 0.16*
^{125}I-βCD-C10-PEG$_{5000}$-NP	1.15 ± 0.35†	0.74 ± 0.13*	1.13 ± 0.14†	0.78 ± 0.12	1.04 ± 0.05†,‡
Liver					
^{125}I-βCD-C10-NP	61.8 ± 7.7	55.1 ± 5.6	65.2 ± 4.8	67.9 ± 4.8	64.4 ± 4.2
^{125}I-βCD-C10-PEG$_{2000}$-NP	82.9 ± 13.7	79.4 ± 6.4*	74.9 ± 3.0	90.1 ± 5.8*	76.0 ± 3.9
^{125}I-βCD-C10-PEG$_{5000}$-NP	63.7 ± 5.6	73.9 ± 3.6	62.5 ± 6.3	75.5 ± 5.5	63.3 ± 4.1
Kidney					
^{125}I-βCD-C10-NP	0.82 ± 0.32	0.48 ± 0.10	0.41 ± 0.16	0.47 ± 0.20	0.18 ± 0.04
^{125}I-βCD-C10-PEG$_{2000}$-NP	0.60 ± 0.05	0.40 ± 0.03	0.28 ± 0.04	0.29 ± 0.02	0.16 ± 0.01
^{125}I-βCD-C10-PEG$_{5000}$-NP	0.52 ± 0.03	0.44 ± 0.02	0.27 ± 0.03	0.25 ± 0.01	0.14 ± 0.02
Brain					
^{125}I-βCD-C10-NP	0.02 ± 0.00	0.01 ± 0.00	0.01 ± 0.00	0.01 ± 0.00	0.00 ± 0.00
^{125}I-βCD-C10-PEG$_{2000}$-NP	0.04 ± 0.00*	0.03 ± 0.00†	0.02 ± 0.00†	0.02 ± 0.00†	0.01 ± 0.00†
^{125}I-βCD-C10-PEG$_{5000}$-NP	0.05 ± 0.00†	0.03 ± 0.00†‡	0.02 ± 0.00†	0.02 ± 0.00*	0.01 ± 0.00†
Heart					
^{125}I-βCD-C10-NP	1.20 ± 0.57	2.19 ± 0.38	0.43 ± 0.13	0.80 ± 0.04	0.32 ± 0.10
^{125}I-βCD-C10-PEG$_{2000}$-NP	0.30 ± 0.01	0.33 ± 0.12*	0.21 ± 0.09	0.17 ± 0.01†	0.12 ± 0.04
^{125}I-βCD-C10-PEG$_{5000}$-NP	0.18 ± 0.05	0.16 ± 0.01*	0.09 ± 0.01	0.08 ± 0.01‡	0.05 ± 0.01
Lung					
^{125}I-βCD-C10-NP	0.39 ± 0.11	0.29 ± 0.03	0.18 ± 0.02	0.23 ± 0.04	0.15 ± 0.02
^{125}I-βCD-C10-PEG$_{2000}$-NP	0.43 ± 0.05	0.31 ± 0.01	0.35 ± 0.05	0.34 ± 0.07	0.28 ± 0.02†
^{125}I-βCD-C10-PEG$_{5000}$-NP	0.32 ± 0.05	0.25 ± 0.01‡	0.16 ± 0.01‡	0.17 ± 0.01	0.08 ± 0.01*‡
Thyroid					
^{125}I-βCD-C10-NP	0.06 ± 0.01	0.23 ± 0.07	0.19 ± 0.11	0.45 ± 0.05	0.50 ± 0.05
^{125}I-βCD-C10-PEG$_{2000}$-NP	0.09 ± 0.01	0.33 ± 0.07	0.69 ± 0.11*	1.46 ± 0.30	1.20 ± 0.23*
^{125}I-βCD-C10-PEG$_{5000}$-NP	0.05 ± 0.01‡	0.23 ± 0.07	0.72 ± 0.30	0.69 ± 0.28	0.83 ± 0.14

Organ activity was expressed as percent injected dose (%ID).
* $P < 0.05$ *vs* βCD-C10-NP.
† $P < 0.01$ *vs* βCD-C10-NP.
‡ $P < 0.05$ *vs* βCD-C10-PEG$_{2000}$-NP.

between compounds at early time points (10 min and 1 h). A significantly higher ^{125}I-βCD-C10-PEG$_{2000}$-NP and ^{125}I-βCD-C10-PEG$_{5000}$-NP blood activity as compared with that of ^{125}I-βCD-C10-NP was observed at later time points (3, 6 and 24 h). Consequently, AUC values for ^{125}I-βCD-C10-PEG$_{2000}$-NP and ^{125}I-βCD-C10-PEG$_{5000}$-NP blood activity were respectively 2.8-fold and 3.4-fold higher than that observed following injection of ^{125}I-βCD-C10-NP. A corresponding graded decrease in splanchnic activity from ^{125}I-βCD-C10-NP to ^{125}I-βCD-C10-PEG$_{2000}$-NP and ^{125}I-βCD-C10-PEG$_{5000}$-NP was observed at all time points, yielding ^{125}I-βCD-C10-PEG$_{2000}$-NP and ^{125}I-βCD-C10-PEG$_{5000}$-NP AUC values that were respectively 2.6-fold and 4.1-fold lower than that observed for ^{125}I-βCD-C10-NP. No significant differences were observed in nanoparticle renal activity. Finally, there was a tendency toward overall higher hepatic activity of ^{125}I-βCD-C10-PEG$_{2000}$-NP as compared with ^{125}I-βCD-C10-NP whereas no significant difference was observed between ^{125}I-βCD-C10-PEG$_{5000}$-NP and ^{125}I-βCD-C10-NP hepatic activity except at 1 h post-injection.

The biodistribution of ^{125}I-βCD-C10-NP, ^{125}I-βCD-C10-PEG$_{2000}$-NP, and ^{125}I-βCD-C10-PEG$_{5000}$-NP in the remaining organs being evaluated is presented in Fig. 4.

There was no major difference between ^{125}I-βCD-C10-NP, ^{125}I-βCD-C10-PEG$_{2000}$-NP, and ^{125}I-βCD-C10-PEG$_{5000}$-NP activities in the bile, stomach, salivary glands, brown adipose tissue, skin, pancreas, and lungs. The cerebral activities of ^{125}I-βCD-C10-PEG$_{2000}$-NP, and ^{125}I-βCD-C10-PEG$_{5000}$-NP were significantly higher than that of ^{125}I-βCD-C10-NP despite overall low brain activity for all 3 nanoparticles. The cardiac, skeletal muscle and white adipose tissue activities of ^{125}I-βCD-C10-NP were higher than those of ^{125}I-βCD-C10-PEG$_{2000}$-NP and ^{125}I-βCD-C10-PEG$_{5000}$-NP. There was a slightly but significantly higher intestinal activity of ^{125}I-βCD-C10-PEG$_{2000}$-NP and ^{125}I-βCD-C10-PEG$_{5000}$-NP than that observed for ^{125}I-βCD-C10-NP. Finally, a favorable, significantly lower lung activity was observed for ^{125}I-βCD-C10-PEG$_{5000}$-NP with respect to those of ^{125}I-βCD-C10-NP and ^{125}I-βCD-C10-PEG$_{2000}$-NP at 24 h following injection while ^{125}I-βCD-C10-PEG$_{2000}$-NP lung activity was significantly higher than those of ^{125}I-βCD-C10-PEG$_{5000}$-NP and ^{125}I-βCD-C10-NP at this late time point.

Selective organ uptake expressed as %ID is presented in Table 3 below. The results confirmed those described above with the addition of thyroid activity values < 1.5% of the injected dose indicating good *in vivo* radiolabeling stability.

3.3. In vivo imaging studies

Representative longitudinal *in vivo* SPECT/CT images obtained at 10 min, 1 h, 3 h, 6 h and 24 h following the injection of ^{125}I-βCD-C10-NP, ^{125}I-βCD-C10-PEG$_{2000}$-NP, and ^{125}I-βCD-C10-PEG$_{5000}$-NP are shown in Fig. 5 below. Hepatic activity was readily observed with all NPs. In accordance with results from *ex vivo* biodistribution studies, interscapular brown adipose tissue uptake of ^{125}I-βCD-C10-NP was identified at all time points. In addition, splanchnic activity was observed following injection of ^{125}I-βCD-C10-NP and increased over time whereas it was not observed on images acquired following injection of ^{125}I-βCD-C10-PEG$_{2000}$-NP and ^{125}I-βCD-C10-PEG$_{5000}$-NP.

3.4. Preliminary toxicity studies

Results from preliminary toxicity studies using βCD-C10-PEG5000-NP are presented in Tables 4 and 5 as well as in Fig. 6. Shown in Table 4

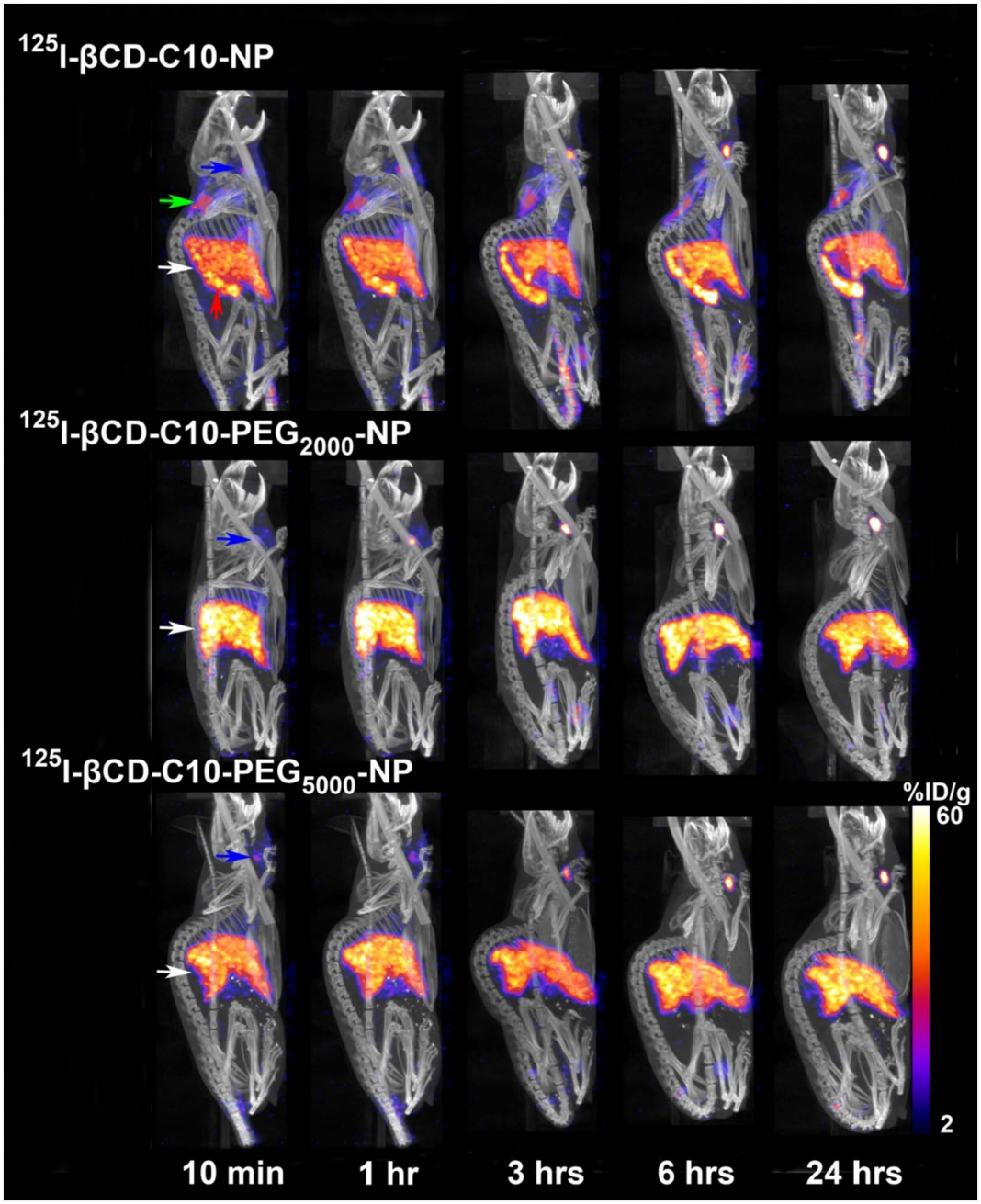

Fig. 5. *In vivo* biodistribution of nanocarriers. Noninvasive *in vivo* SPECT/CT longitudinal imaging of ^{125}I-βCD-C10, ^{125}I-βCD-C10-PEG$_{2000}$, and ^{125}I-βCD-C10-PEG$_{5000}$ whole-body distribution at 10 min, 1 h, 3 h, 6 h, and 24 h following intravenous injection in representative animals. White, red, green, and blue arrows on 10 min images respectively point to liver, spleen, BAT, and thyroid activity. (For interpretation of the references to colour in this figure legend, the reader is referred to the web version of this article.)

are whole body and major organ weights of animals injected with saline (CTL) or βCD-C10-PEG$_{5000}$-NP thrice a week for 2 weeks at 3 and 30 days following treatment completion. The whole body weight of βCD-C10-PEG$_{5000}$-NP-treated animals significantly increased between day 3 and day 30 following treatment completion and was significantly higher than that of control animals. There were 25 and 70% increases in day 30- hepatic and day 3-splanchnic weights of βCD-C10-PEG$_{5000}$-NP-treated animals as compared with that of CTL animals ($P < 0.05$).

As shown in Table 5 below, blood cell counts revealed no significant differences in hematocrit nor in erythrocyte, thrombocyte, and leukocyte counts between CTL and βCD-C10-PEG$_{5000}$-NP -treated animals. Serum creatinine and ALT levels at day 3 and day 30 following treatment completion were not significantly different in βCD-C10-PEG$_{5000}$-NP-treated animals when compared with the CTL group.

Representative histological images of renal, splanchnic, and hepatic samples from CTL and βCD-C10-PEG$_{5000}$-NP-treated animals at day 3 and day 30 following treatment are shown in Fig. 6 below. The results indicated that no distinctive histological features were observed on kidney and spleen samples from βCD-C10-PEG$_{5000}$-NP-treated animals as compared with CTL. Multiple small, non-necrotizing portal or intraparenchymal granulomas were observed on hepatic samples. Granulomas consisted of aggregates of epithelioid histiocytes as well as inflammatory cells. The density of granulomas was higher at day 3 than at day 30 following treatment.

4. Discussion

The main results of the present study were that βCD-C10-PEG$_{5000}$-

Table 4
Whole body and major organ weights of CD1 mice injected with saline (CTL) or βCD-C10-PEG_{5000}-NP.

	CTL	βCD-C10-PEG_{5000}-NP
Whole body		
Day 3	28.5 ± 1.0	28.6 ± 1.2
Day 30	31.8 ± 1.6	37.1 ± 1.6*†
Brain		
Day 3	0.50 ± 0.01	0.48 ± 0.01
Day 30	0.52 ± 0.00†	0.52 ± 0.01
Heart		
Day 3	0.12 ± 0.00	0.12 ± 0.00
Day 30	0.14 ± 0.01†	0.13 ± 0.00†
Liver		
Day 3	1.41 ± 0.06	1.71 ± 0.13
Day 30	1.55 ± 0.06	1.95 ± 0.10*
Ovaries		
Day 3	0.012 ± 0.001	0.014 ± 0.002
Day 30	0.020 ± 0.003†	0.019 ± 0.005
Spleen		
Day 3	0.11 ± 0.01	0.19 ± 0.03*
Day 30	0.10 ± 0.01	0.20 ± 0.04
Kidneys		
Day 3	0.32 ± 0.01	0.35 ± 0.01
Day 30	0.35 ± 0.01†	0.39 ± 0.01

* $P < 0.05$ *vs* CTL.
† $P < 0.05$ *vs* Day 3.

Table 5
Blood cell and serum creatinine analysis of CD1 mice at day 3 and day 30 following treatment with saline (CTL) or βCD-C10-PEG5000-NP.

	CTL	βCD-C10-PEG_{5000}-NP
Hematocrit (% volume)		
Day 3	43.9 ± 1.3	41.8 ± 0.9
Day 30	43.2 ± 1.0	43.5 ± 0.6
Erythrocytes ($10^5 \cdot \mu L^{-1}$)		
Day 3	75.6 ± 3.7	71.2 ± 2.4
Day 30	73.5 ± 3.2	79.4 ± 4.4
Thrombocytes ($10^5 \cdot \mu L^{-1}$)		
Day 3	7.3 ± 0.6	5.4 ± 0.9
Day 30	7.0 ± 0.6	7.4 ± 0.6
Leukocytes ($10^5 \cdot \mu L^{-1}$)		
Day 3	0.026 ± 0.005	0.036 ± 0.005
Day 30	0.028 ± 0.003	0.025 ± 0.007
Creatinine ($\mu mol \cdot L^{-1}$)		
Day 3	66.0 ± 11.3	86.6 ± 18.9
Day 30	113.6 ± 26.0	67.1 ± 12.2
ALT ($U \cdot L^{-1}$)		
Day 3	3.7 ± 1.0	4.2 ± 0.3
Day 30	8.9 ± 2.8	8.1 ± 3.6

See Materials & methods for treatment details. ALT, alanine aminotransferase.

NP systems displayed improved stealthiness following *in vivo* intravenous injection with reduced elimination and increased circulating concentration in comparison with βCD-C10-PEG_{2000}-NP and βCD-C10-NP. In addition, repeated βCD-C10-PEG_{5000}-NP administration did not result in organ toxicity in preliminary acute and extended acute toxicity studies.

Nanoparticle suspensions were obtained by the solvent displacement methodology [26]. An organic/water phase ratio of 1/3 was finally selected for the formulations since it favored smaller sized (~50 nm) nanoparticles. A 1:1 βCD-C10/^{125}I-βCD-C10 ratio was used in the present study for the formulation of ^{125}I-βCD-C10-NPs, ^{125}I-βCD-C10-PEG_{2000}-NPs and ^{125}I-βCD-C10-PEG_{5000}-NPs. The (1:1) ratio was also selected on the basis of previously published results [23]. The iodinated nanoparticles (^{125}I-βCD-C10-NP) had mean size and zeta potential values similar to those of non-iodinated nanoparticles βCD-C10-NP. Moreover, ^{125}I-βCD-C10-NP presented a monodisperse distribution (PI of 0.12) indicating that the two derivatives co-assembled during the formulation step. The NPs were surface-decorated by co-nanoprecipitating the bioesterified βCD with PEGylated phospholipids with PEG chain lengths of 2000 and 5000 Da [20]. ^{125}I-βCD-C10-PEG_{2000}-NPs and ^{125}I-βCD-C10-PEG_{5000}-NPs displayed good colloidal stability in electrolytes, which was better than that of ^{125}I-βCD-C10-NP. Good electrolyte stability together with a moderate increase in average diameter and a change of zeta potential absolute values were in favor of the presence of the hydrophilic PEG corona, ensuring a steric hindrance at the surface of the nanoparticles preventing flocculation.

The removal of NPs from the bloodstream occurs mainly through NP opsonization preceding and allowing the binding and phagocytosis of NPs by mononuclear phagocytes from the mononuclear phagocytic system (MPS) [27,28]. A potential lack of significant NP degradation by phagocytes following ingestion leads in turn to NP sequestration in organ of the MPS. Our results indicated that NPs used in the present study behaved in accordance with such a general scheme, with the liver and spleen being the tissues with higher NP activity following intravenous injection as indicated by *ex vivo* biodistribution as well as *in vivo* nuclear imaging data. In addition, undecorated ^{125}I-βCD-C10-NP blood removal occurred within a time range of seconds to minutes as shown by the major differences in circulating activity that were observed between ^{125}I-βCD-C10-NP and ^{125}I-βCD-C10-PEG_{2000}-NP/^{125}I-βCD-C10-PEG_{5000}-NP as soon as the earliest time point of 10 min following intravenous injection. NP decoration with PEG increased their blood concentration over time, with several-fold higher ^{125}I-βCD-C10-PEG_{2000}-NP and ^{125}I-βCD-C10-PEG_{5000}-NP AUC values with respect to that of undecorated ^{125}I-βCD-C10-NPs and a corresponding decrease in the splanchnic exposition to ^{125}I-βCD-C10-PEG_{2000}-NP and ^{125}I-βCD-C10-PEG_{5000}-NP when compared to that of undecorated NPs.

Poly(ethylene glycol) (PEG) grafting is a widely used method for increasing the stealthiness of intravenously injected nanoparticles [29,30]. The mechanisms by which PEG chains reduce opsonization and therefore elimination of NPs might involve the modification of PEG chain conformation from extended to compress when opsonins interact with NPs. Compression of PEG chain conformation would generate repulsive forces that ideally would counterbalance or exceed the attractive interactions leading to opsonin binding to the NP surface [27]. In the present study, PEG chains with molecular weights of 2000 and 5000 Da were evaluated since previous studies have shown a graded decrease in plasma protein adsorption on NPs from 2000 to 5000 Da PEG chains with no further reduction with PEG chains of higher M_W [31]. The greater decrease in opsonization with PEG chains of higher M_W might be related to the fact that PEG M_W is proportional to PEG chain length, with higher chain length allowing higher nanoparticle surface shielding with improved *in vitro* protection from opsonization and blood removal [32,33]. Our *in vivo* results therefore confirmed these previously published *in vitro* data.

Unlike what was observed in the spleen, the NP liver activity was not significantly affected by the presence or absence of PEG_{2000} and PEG_{5000}. Organ-specific opsonins have been described which preferentially target opsonized particles to hepatic or splanchnic phagocytic cells [34,35]. Our results indicating a reduced splanchnic activity and a simultaneously modest if any improvement of hepatic activity with PEG decoration of NP therefore suggest that ^{125}I-βCD-C10-NPs might be predominantly recognized by spleen-specific opsonins.

In addition to blood and splanchnic activities, PEG_{5000} decoration also led to an improved lung activity with respect to undecorated and PEG_{2000}-decorated NPs. As lung accumulation of NP frequently occurs as a consequence of NP aggregation and physical obstruction of the pulmonary capillary bed [33], our results therefore suggest that ^{125}I-βCD-C10-PEG_{5000}-NPs might be less amenable to aggregation than ^{125}I-β-CD-C10-NPs and ^{125}I-βCD-C10-PEG_{2000}-NPs.

Finally, an additional interesting and specific feature of ^{125}I-βCD-C10-NP biodistribution is the significantly higher radioactivity found in the cardiac, skeletal muscle, and white adipose tissues in comparison with PEG-decorated NPs. Such tissues are significantly using

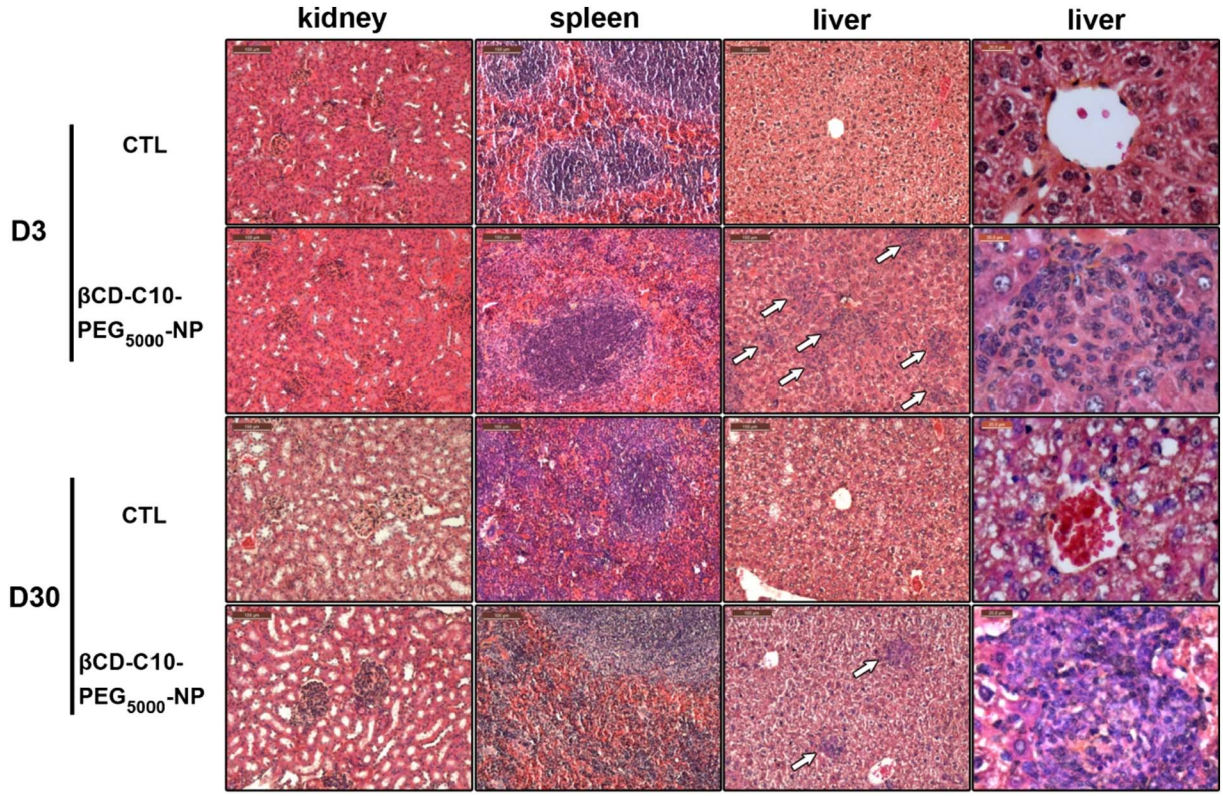

Fig. 6. Histological analysis from preliminary acute and extended acute toxicity studies. HES (hematoxylin, eosin, saffron) histological staining of kidney, spleen, and liver mouse samples at 3 and 30 days following treatment with βCD-C10-PEG_{5000} or vehicle (CTL) (see Materials & methods for details).

carbohydrates as metabolic substrates for energy production and β-CDs used for the formulation of NPs in the present study have been previously shown to be metabolized in a slower but similar way than glucose [36]. The myocardium, skeletal muscle, and white adipose tissue might therefore be involved in ^{125}I-βCD-C10-NP metabolism, in which case the presence of PEG shielding seems to provide protection from such metabolic degradation.

The NP accumulation in MPS organs consecutive to NP blood removal might lead to toxicity despite the increased stealthiness allowed by PEGylation and decreased opsonization. In addition, increased circulating concentrations of NPs due to improved stealthiness might lead to blood cell cytotoxicity as well. Preliminary toxicity studies were therefore performed using βCD-C10-PEG_{5000}-NPs in accordance with their favorable biodistribution properties as indicated by the *in vivo* studies discussed above.

Preliminary acute (3 days) and extended acute (30 days) toxicity studies were performed using a total injected dose of ~150 mg/kg of βCD-C10-PEG_{5000}-NPs. The dose and volume were defined considering the upper limit of βCD-C10-PEG_{5000}-NPs solubility (2.6 mg/mL) on one hand, and the maximum volume to be injected while adhering to good practices on the other hand [37]. The resulting dose falls within the range of doses classically used while evaluating the potential toxicity of nanoparticles [38]. The exposure of mice to such a dose did not result in kidney histological abnormalities, which was confirmed by the lack of alteration in renal function as approximated by creatinine serum level assay. Indeed, βCD-C10-PEG_{5000}-NP hydrodynamic diameter (66 ± 2 nm) is above the size limit under which particle size is low enough to allow kidney filtration [39]. Similarly, no significant variation in blood cell counts was observed. Spleen accumulation of βCD-C10-PEG_{5000}-NPs, which was minimized with respect to that observed following injection of βCD-C10-NPs and βCD-C10-PEG_{2000}-NPs, did not induce any specific histological feature. Finally, the histological analysis of hepatic samples from βCD-C10-PEG_{5000}-NP-treated animals indicated the involvement of the MPS at the portal and parenchymal levels as indicated by the presence of histiocytes at these anatomic locations. These histological results are well in accordance with *ex vivo* and *in vivo* biodistribution data indicating preferential hepatic elimination of radiolabeled ^{125}I-βCD-C10-PEG_{5000}-NPs. However, the involvement of the MPS following high dose administration of βCD-C10-PEG_{5000}-NPs remained in the physiological range as indicated by comparable ALT serum levels in control and βCD-C10-PEG_{5000}-NP-treated animals. In addition, the qualitative analysis of histological hepatic stainings also revealed that the density of histiocytes-containing granulomas decreased from 3 to 30 days following βCD-C10-PEG_{5000}-NP treatment. Overall, high dose βCD-C10-PEG_{5000}-NP administration did not result in acute or extended acute tissue toxicity.

5. Conclusions

The decoration of self-assembled βCD-C10 NPs with PEG_{2000} and PEG_{5000} resulted in increased stealthiness *in vivo* with significantly reduced blood clearance and splanchnic activity as observed from *ex vivo* biodistribution and *in vivo* SPECT imaging following radiolabeling and nuclear imaging. ^{125}I-β-CD-C10-PEG_{5000} NPs displayed the most favorable *in vivo* properties without causing organ toxicity in the experimental conditions used in our study. The potential of βCD-C10-PEG_{5000} NPs as drug nanocarriers is under current evaluation.

Conflicts of interest

None.

Acknowledgements

This work was supported by Agence Nationale de la Recherche (CYDEXCAR: ANR-11-BS10-0007), Labex ARCANE (ANR-11-LABX-0003-01) and Institut de Chimie Moléculaire de Grenoble (FR 2607). We thank the NanoBio-ICMG platform for granting access to the

electron microscopy facility.

References

[1] R. Duncan, R. Gaspar, Nanomedicine(s) under the microscope, Mol. Pharm. 8 (6) (2011) 2101–2141.
[2] L.H. Reddy, D. Bazile, Drug delivery design for intravenous route with integrated physicochemistry, pharmacokinetics and pharmacodynamics: illustration with the case of taxane therapeutics, Adv. Drug Deliv. Rev. 71 (2014) 34–57.
[3] G. Calixto, J. Bernegossi, B. Fonseca-Santos, M. Chorilli, Nanotechnology-based drug delivery systems for treatment of oral cancer: a review, Int. J. Nanomedicine 9 (2014) 3719–3735.
[4] H. Leemhuis, R.M. Kelly, L. Dijkhuizen, Engineering of cyclodextrin glucanotransferases and the impact for biotechnological applications, Appl. Microbiol. Biotechnol. 85 (4) (2010) 823–835.
[5] M.E. Davis, M.E. Brewster, Cyclodextrin-based pharmaceutics: past, present and future, Nat. Rev. Drug Discov. 3 (12) (2004) 1023–1035.
[6] R. Challa, A. Ahuja, J. Ali, R.K. Khar, Cyclodextrins in drug delivery: an updated review, AAPS PharmSciTech 6 (2) (2005) E329–57.
[7] S. Shimpi, B. Chauhan, P. Shimpi, Cyclodextrins: application in different routes of drug administration, Acta Pharm. (Zagreb, Croatia) 55 (2) (2005) 139–156.
[8] T. Loftsson, D. Duchene, Cyclodextrins and their pharmaceutical applications, Int. J. Pharm. 329 (1–2) (2007) 1–11.
[9] A.R. Katageri, M.A. Sheikh, Cyclodextrin a gift to pharmaceutical world (review), Int. Res. J. Pharm. 3 (1) (2012) 52–56.
[10] T. Loftsson, M.E. Brewster, Cyclodextrins as functional excipients: methods to enhance complexation efficiency, J. Pharm. Sci. 101 (9) (2012) 3019–3032.
[11] J. Zhang, P.X. Ma, Cyclodextrin-based supramolecular systems for drug delivery: recent progress and future perspective, Adv. Drug Deliv. Rev. 65 (9) (2013) 1215–1233.
[12] J.R. Lakkakula, R.W. Macedo Krause, A vision for cyclodextrin nanoparticles in drug delivery systems and pharmaceutical applications, Nanomedicine (Lond.) 9 (6) (2014) 877–894.
[13] L. Zerkoune, A. Angelova, S. Lesieur, Nano-assemblies of modified cyclodextrins and their complexes with guest molecules: incorporation in nanostructured membranes and amphiphile nanoarchitectonics design, Nano 4 (3) (2014) 741–765.
[14] J.B.G. Yameogo, A. Gèze, L. Choisnard, J.L. Putaux, R. Semdé, D. Wouessidjewe, Progress in developing amphiphilic cyclodextrin-based nanodevices for drug delivery, Curr. Top. Med. Chem. (Sharjah, United Arab Emirates) 14 (4) (2014) 526–541.
[15] V. Bonnet, C. Gervaise, F. Djedaïni-Pilard, A. Furlan, C. Sarazin, Cyclodextrin nanoassemblies: a promising tool for drug delivery, Drug Discov. Today 20 (9) (2015) 1120–1126.
[16] L. Choisnard, A. Gèze, J.L. Putaux, Y.S. Wong, D. Wouessidjewe, Nanoparticles of Î²-Cyclodextrin esters obtained by self-assembling of biotransesterified Î²-Cyclodextrins, Biomacromolecules 7 (2) (2006) 515–520.
[17] L. Choisnard, A. Gèze, B.G. Yaméogo, J.L. Putaux, D. Wouessidjewe, Miscellaneous nanoaggregates made of Î²-CD esters synthesized by an enzymatic pathway, Int. J. Pharm. 344 (1–2) (2007) 26–32.
[18] A. Gèze, L. Choisnard, J.L. Puteaux, D. Wouessidjewe, Colloidal systems made of biotransesterified α-, β-, and γ-cyclodextrins grafted with C10 alkyl chains, Mater. Sci. Eng. C 29 (2) (2009) 458–462.
[19] O. Arnaud, A. Boumendjel, A. Gèze, M. Honorat, E.L. Matera, J. Guitton, W.D. Stein, S.E. Bates, P. Falson, C. Dumontet, A. Di Pietro, L. Payen, The acridone derivative MBLI-87 sensitizes breast cancer resistance protein-expressing xenografts to irinotecan, Eur. J. Cancer 47 (4) (2011) 640–648.
[20] J.B.G. Yaméogo, A. Gèze, L. Choisnard, J.L. Putaux, A. Gansané, S.B. Sirima, R. Semdé, D. Wouessidjewe, Self-assembled biotransesterified cyclodextrins as artemisinin nanocarriers - I: formulation, lyoavailability and in vitro antimalarial activity assessment, Eur. J. Pharm. Biopharm. 80 (3) (2012) 508–517.
[21] J.B.G. Yaméogo, A. Gèze, L. Choisnard, J.L. Putaux, R. Mazet, C. Passirani, M. Keramidas, J.L. Coll, N. Lautram, J. Bejaud, R. Semdé, D. Wouessidjewe, Self-assembled biotransesterified cyclodextrins as potential artemisinin nanocarriers. II: in vitro behavior toward the immune system and in vivo biodistribution assessment of unloaded nanoparticles, Eur. J. Pharm. Biopharm. 88 (3) (2014) 683–694.
[22] L. Choisnard, A. Gèze, C. Vanhaverbeke, J.B. Yaméogo, J.L. Putaux, B. Brasme, L. Jullien, S. Boullanger, C. Elfakir, D. Wouessidjewe, Physicochemical characterization of α-, β-, and γ-cyclodextrins bioesterified with decanoate chains used as building blocks of colloidal nanoparticles, Biomacromolecules 12 (8) (2011) 3031–3038.
[23] A. Gèze, L.T. Chau, L. Choisnard, J.P. Mathieu, D. Marti-Batlle, L. Riou, J.L. Putaux, D. Wouessidjewe, Biodistribution of intravenously administered amphiphilic beta-cyclodextrin nanospheres, Int. J. Pharm. 344 (1–2) (2007) 135–142.
[24] B. Davies, T. Morris, Physiological parameters in laboratory animals and humans, Pharm. Res. 10 (7) (1993) 1093–1095.
[25] A. Gèze, J.L. Putaux, L. Choisnard, P. Jéhan, D. Wouessidjewe, Long-term shelf stability of amphiphilic beta-cyclodextrin nanosphere suspensions monitored by dynamic light scattering and cryo-transmission electron microscopy, J. Microencapsul. 21 (6) (2004) 607–613.
[26] L. Choisnard, A. Géze, M. Bigan, J.L. Putaux, D. Wouessidjewe, Efficient size control of amphiphilic cyclodextrin nanoparticles through a statistical mixture design methodology, J. Pharm. Pharm. Sci. 8 (3) (2005) 593–601.
[27] D.E. Owens 3rd, N.A. Peppas, Opsonization, biodistribution, and pharmacokinetics of polymeric nanoparticles, Int. J. Pharm. 307 (1) (2006) 93–102.
[28] A. Vonarbourg, C. Passirani, P. Saulnier, J.P. Benoit, Parameters influencing the stealthiness of colloidal drug delivery systems, Biomaterials 27 (24) (2006) 4356–4373.
[29] F. Alexis, E. Pridgen, L.-K. Molnar, O.-C. Farokhzad, Factors affecting the clearance and biodistribution of polymeric nanoparticles, Mol. Pharm. 5 (4) (2012) 505–515.
[30] L. Basile, C. Passirani, N. Huynh, J. Béjaud, J.-P. Benoit, G. Puglisi, R. Pignatello, Serum-stable, long-circulating paclitaxel-loaded colloidal carriers decorated with a new amphiphilic PEG derivative, Int. J. Pharm. 426 (2012) 231–238.
[31] R. Gref, M. Lück, P. Quellec, M. Marchand, E. Dellacherie, S. Harnisch, T. Blunk, R.H. Müller, Stealth corona-core nanoparticles surface modified by polyethylene glycol (PEG): influences of the corona (PEG chain length and surface density) and of the core composition on phagocytic uptake and plasma protein adsorption, Colloids Surf. B: Biointerfaces 18 (3–4) (2000) 301–313.
[32] M. Miteva, K.C. Kirkbride, K.V. Kilchrist, T.A. Werfel, H. Li, C.E. Nelson, M.K. Gupta, T.D. Giorgio, C.L. Duvall, Tuning PEGylation of mixed micelles to overcome intracellular and systemic siRNA delivery barriers, Biomaterials 38 (2015) 97–107.
[33] J.S. Suk, Q. Xu, N. Kim, J. Hanes, Ensign LM.PEGylation as a strategy for improving nanoparticle-based drug and gene delivery, Adv. Drug Deliv. Rev. 99 (Pt A) (2016) 28–51.
[34] S.M. Moghimi, H.M. Patel, Tissue specific opsonins for phagocytic cells and their different affinity for cholesterol-rich liposomes, FEBS Lett. 233 (1) (1988) 143–147.
[35] S.M. Moghimi, H.M. Patel, Differential properties of organ-specific serum opsonins for liver and spleen macrophages, Biochim. Biophys. Acta 984 (3) (1989) 379–383.
[36] A. Gerlóczy, A. Fónagy, P. Keresztes, L. Perlaky, J. Szejtli, Absorption, distribution, excretion and metabolism of orally administered 14C-beta-cyclodextrin in rat, Arzneimittelforschung 35 (7) (1985) 1042–1047.
[37] K.H. Diehl, R. Hull, D. Morton, R. Pfister, Y. Rabemampianina, D. Smith, J.M. Vidal, C. van de Vorstenbosch, European Federation of Pharmaceutical Industries Association and European Centre for the Validation of Alternative Methods. A good practice guide to the administration of substances and removal of blood, including routes and volumes, J. Appl. Toxicol. 21 (1) (2001) 15–23.
[38] S. Kanakia, J.D. Toussaint, S. Mullick Chowdhury, T. Tembulkar, S. Lee, Y.P. Jiang, R.Z. Lin, K.R. Shroyer, W. Moore, B. Sitharaman, Dose ranging, expanded acute toxicity and safety pharmacology studies for intravenously administered functionalized graphene nanoparticle formulations, Biomaterials 35 (25) (2014) 7022–7031.
[39] H.S. Choi, W. Liu, P. Misra, E. Tanaka, J.P. Zimmer, B. Itty Ipe, M.G. Bawendi, J.V. Frangioni, Renal clearance of nanoparticles, Nat. Biotechnol. 25 (10) (2007) 1165–1170.
[40] L. Choisnard, A. Gèze, C. Vanhaverbeke, J.B Yaméogo, J.L Putaux, B. Brasme, L. Jullien, S. Boullanger, C. Elfakir, D. Wouessidjewe, Physicochemical Characterization of alpha-, beta-, and gamma-Cyclodextrins Bioesterified with Decanoate Chains Used As Building Blocks of Colloidal Nanoparticles, Biomacromolecules 12 (8) (2011) 3031–3038.